

Supplementary Materials for

Revealing hidden supercooled liquid states in Al-based metallic glasses by ultrafast scanning calorimetry: Approaching the theoretical ceiling of liquid fragility

Qun Yang¹, Jing Huang², Xiao-Hui Qin¹, Fa-Xi Ge¹, and Hai-Bin Yu^{1}*

¹ Wuhan National High Magnetic Field Center and School of Physics, Huazhong University of Science and Technology, WuHan 430074, China

² School of Materials and Engineering, Huazhong University of Science and Technology, Wuhan 430074, China

The Supplementary Materials provides details on the following five aspects of the work:

1. Verified accuracy of liquid fragility measured by FSC in three ways for Al-based MGs;
2. The heat flow curves of the twenty Al-based MGs by FSC at different heating rates, and determination of the liquid fragility for the twenty Al-based MGs;
3. Detailed data about glass forming ability;
4. Determination of the crystal melting temperature and the liquid temperature from DTA data;
5. The database of liquid fragility and glass transition temperature for different glass formers with different bonding nature.

1. Verification of the accuracy of the liquid fragility was performed by FSC.

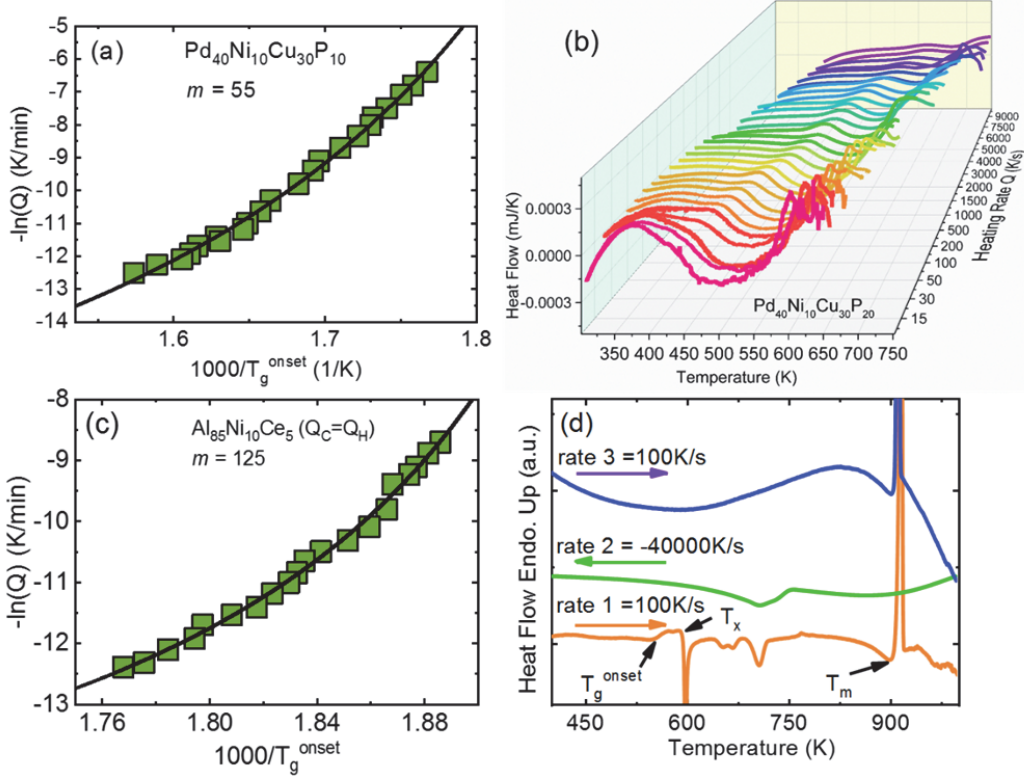


Figure S1. (a) The onset temperature of glass transition, T_g^{onset} , vs heating rates for a $\text{Pd}_{40}\text{Ni}_{30}\text{Cu}_{10}\text{P}_{10}$ MG. The black solid line is a fit using the VFT equation. (b) Heat flow curves measured by FSC using different heating rates for a $\text{Pd}_{40}\text{Ni}_{30}\text{Cu}_{10}\text{P}_{10}$ MG. (c) The glass transition kinetics is analyzed in terms of a VFT type equation for describing the heating rate dependence of the glass transition onset temperature for $\text{Al}_{85}\text{Ni}_{10}\text{Ce}_5$ MG at various heating rates Q_H from 50 to 4000 K/s where $Q_H=Q_C$. (d) The glass forming ability of $\text{Al}_{85}\text{Ni}_{10}\text{Ce}_5$ MG have been measured at different a series of three heating/cooling cycles on a MultiSTAR UFH 1 MEMS chip sensor. Here, for the first time, Flash DSC reaching heating rates of 100 K/s (rate 1) is utilized to investigate the thermal behavior of $\text{Al}_{85}\text{Ni}_{10}\text{Ce}_5$ MG up to the liquid temperature. It is obvious that the

$\text{Al}_{85}\text{Ni}_{10}\text{Ce}_5$ MG clearly undergoes a transformation from an amorphous state to a crystalline state through an undercooled liquid region and a series of exothermic crystallization reaction, and the sample eventually melts into a liquid state. Here, we can obtain the heat capacity jump at T_g and the enthalpy of melting. Subsequently, the melted liquid was cooled down at a cooling rate of 40,000 K/s (rate 2), and it was found that the sample crystallized at about 750 K during the cooling. Subsequent heating of the cooled sample again at a heating rate of 100 K/s (rate 3) further demonstrates that $\text{Al}_{85}\text{Ni}_{10}\text{Ce}_5$ MG has a higher critical cooling rate than 40,000 K/s.

2. The heat flow curves of the twenty Al-based MGs by FSC at different heating rates, and determination of the liquid fragility for the twenty Al-based MGs.

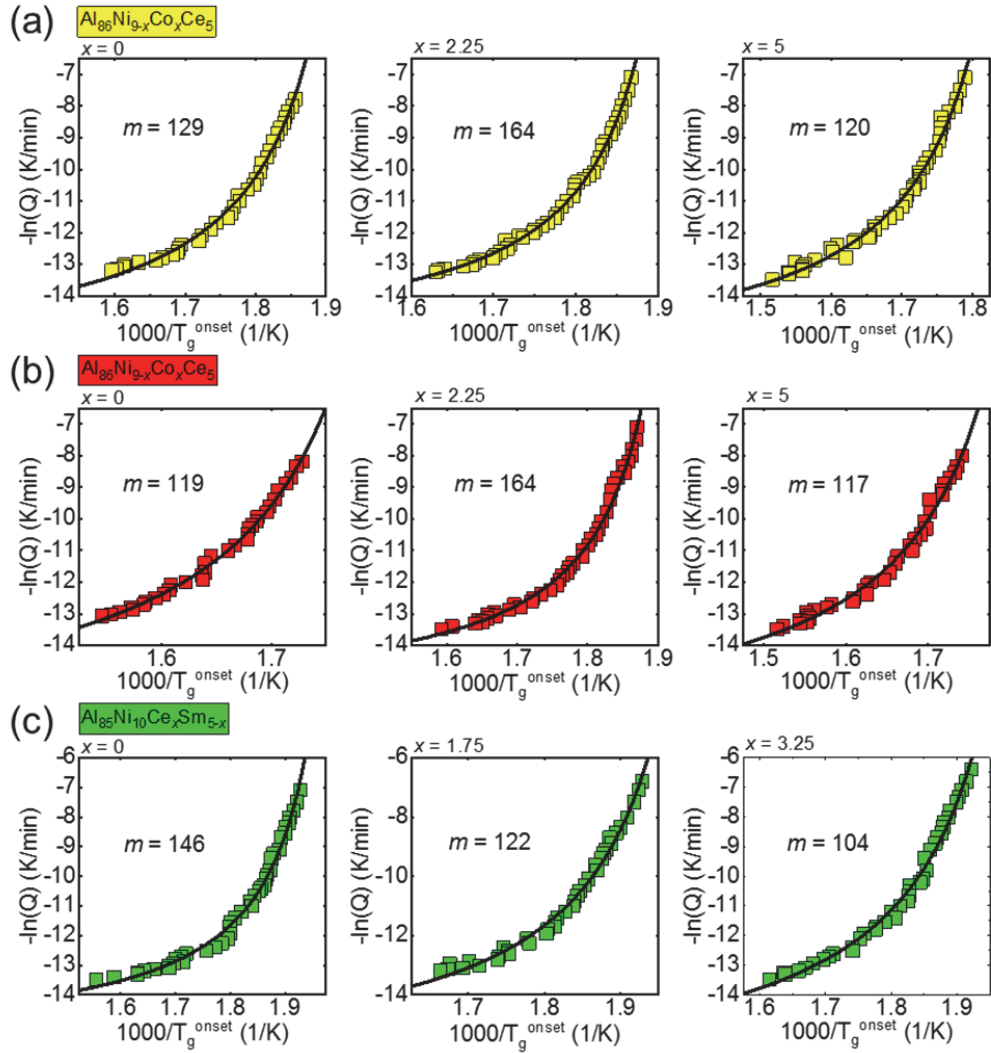


Figure S2. The onset temperature of glass transition, T_g^{onset} , vs heating rates for different Al-based MGs **(a)** $\text{Al}_{86}\text{Ni}_{9-x}\text{Co}_x\text{Ce}_5$ ($x=0, 2.25, 5$ at.%); **(b)** $\text{Al}_{86}\text{Ni}_{9-x}\text{Co}_x\text{La}_5$ ($x=0, 2.25, 5$ at.%); **(c)** $\text{Al}_{85}\text{Ni}_{10}\text{Ce}_x\text{Sm}_{5-x}$ ($x=0, 1.75, 3.25$ at.%). The black solid line is a fit using the VFT equation.

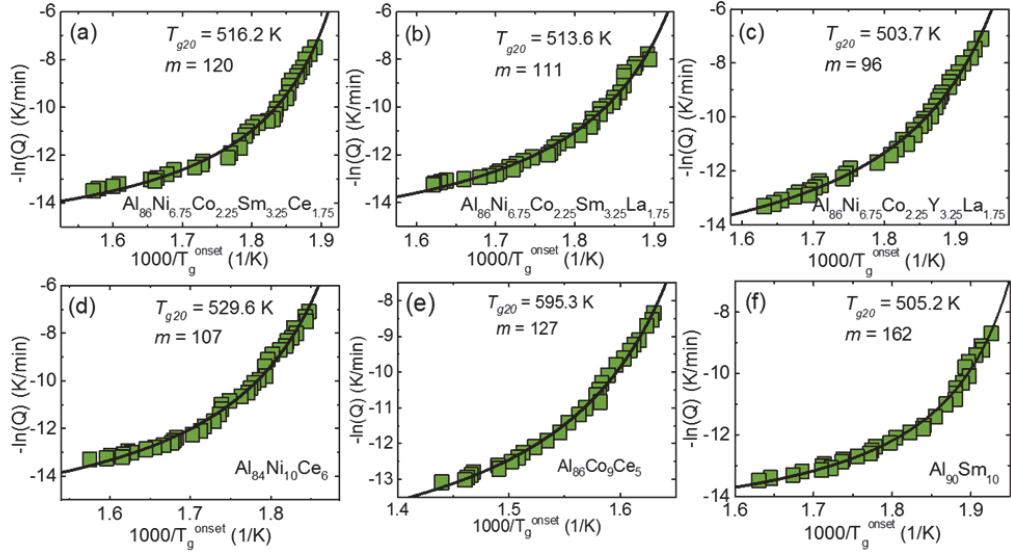


Figure S3. The onset temperature of glass transition, T_g^{onset} , vs heating rates for different Al-based MGs **(a)** Al₈₆Ni_{6.75}Co_{2.25}Sm_{3.25}Ce_{1.75}; **(b)** Al₈₆Ni_{6.75}Co_{2.25}Sm_{3.25}La_{1.75}; **(c)** Al₈₆Ni_{6.75}Co_{2.25}Y_{3.25}La_{1.75}; **(d)** Al₈₄Ni₁₀Ce₆; **(e)** Al₈₆Co₉Ce₅; **(f)** Al₉₀Sm₁₀. The black solid line is a fit using the VFT equation. The T_{g20} is extrapolated from the FSC data.

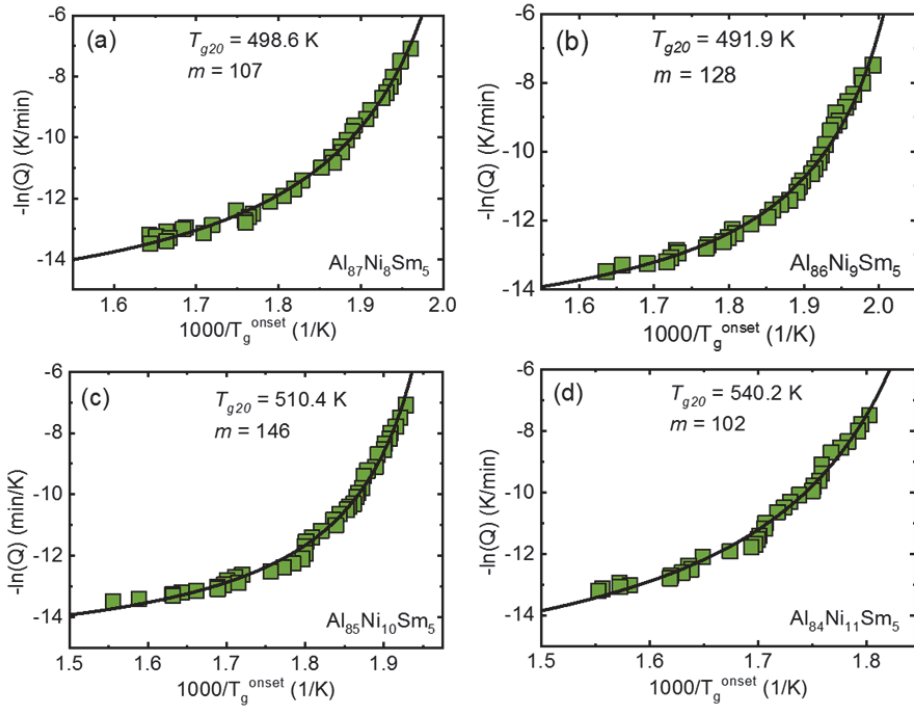


Figure S4. The onset temperature of glass transition, T_g^{onset} , vs heating rates for the $\text{Al}_{95-x}\text{Ni}_x\text{Sm}_5$ ($x=8$ (a), 9 (b), 10 (c), 11 (d) at.%) MGs. The black solid line is a fit using the VFT equation. The T_{g20} is extrapolated from the FSC data.

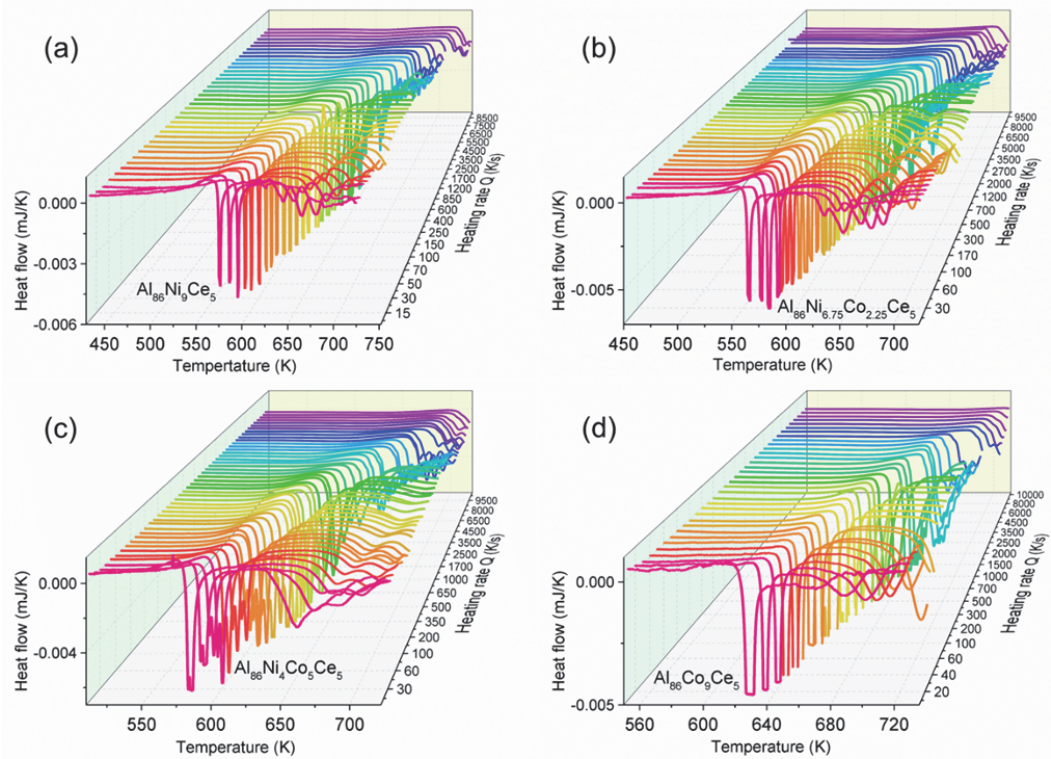


Figure S5. Heat flow curves are measured by FSC using different heating rates from 10-10000 K/s for Al₈₆Ni_{9-x}Co_xCe₅ ($x=0$ (a), 2.25 (b), 5 (c), 9 (d) at.%) MGs. The heat flow curves for different heating rates are normalized by dividing by the heating rate.

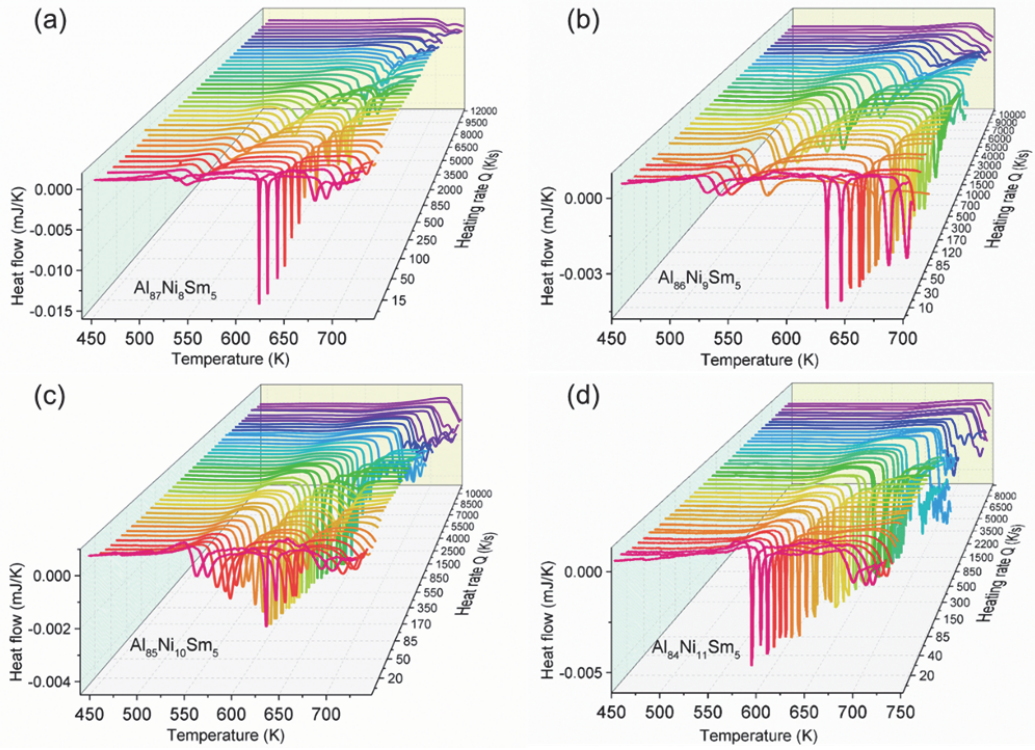


Figure S6. Heat flow curves are measured by FSC using different heating rates from 10-12000 K/s for $\text{Al}_{95-x}\text{Ni}_x\text{Sm}_5$ ($x=8$ (a), 9 (b), 10 (c), 11 (d) at.%) MGs.

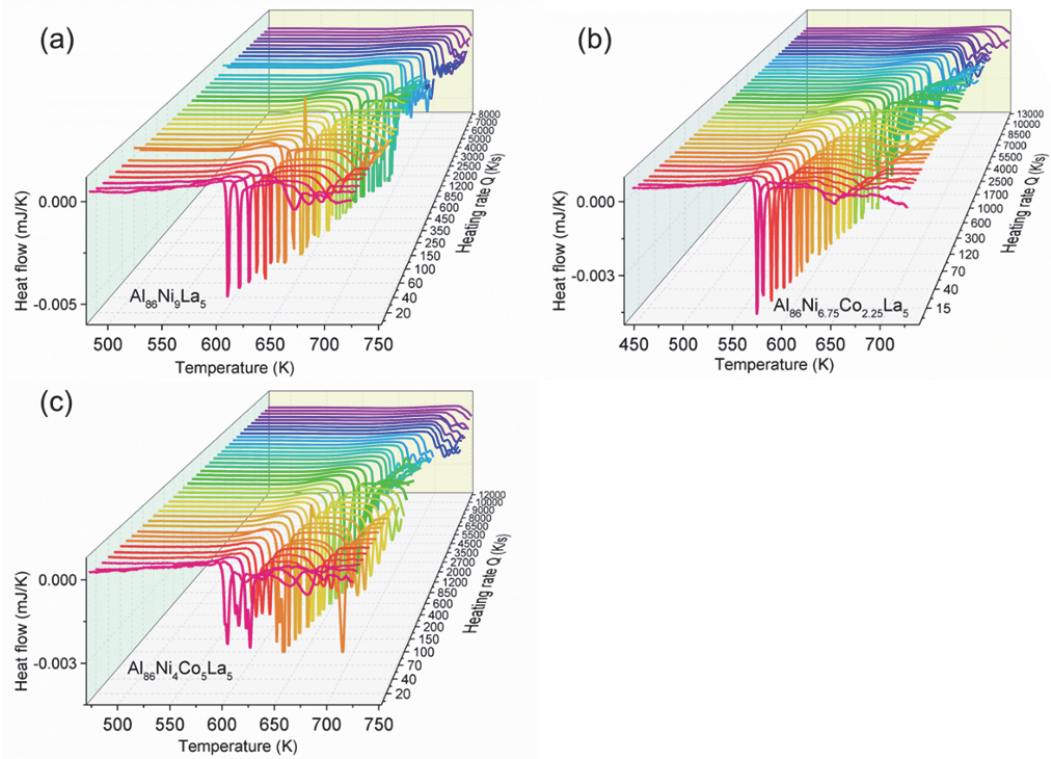


Figure S7. Heat flow curves are measured by FSC using different heating rates from 10-13000 K/s for $\text{Al}_{86}\text{Ni}_{9-x}\text{Co}_x\text{La}_5$ ($x=0$ (a), 2.25 (b), 5 (c) at.%) MGs.

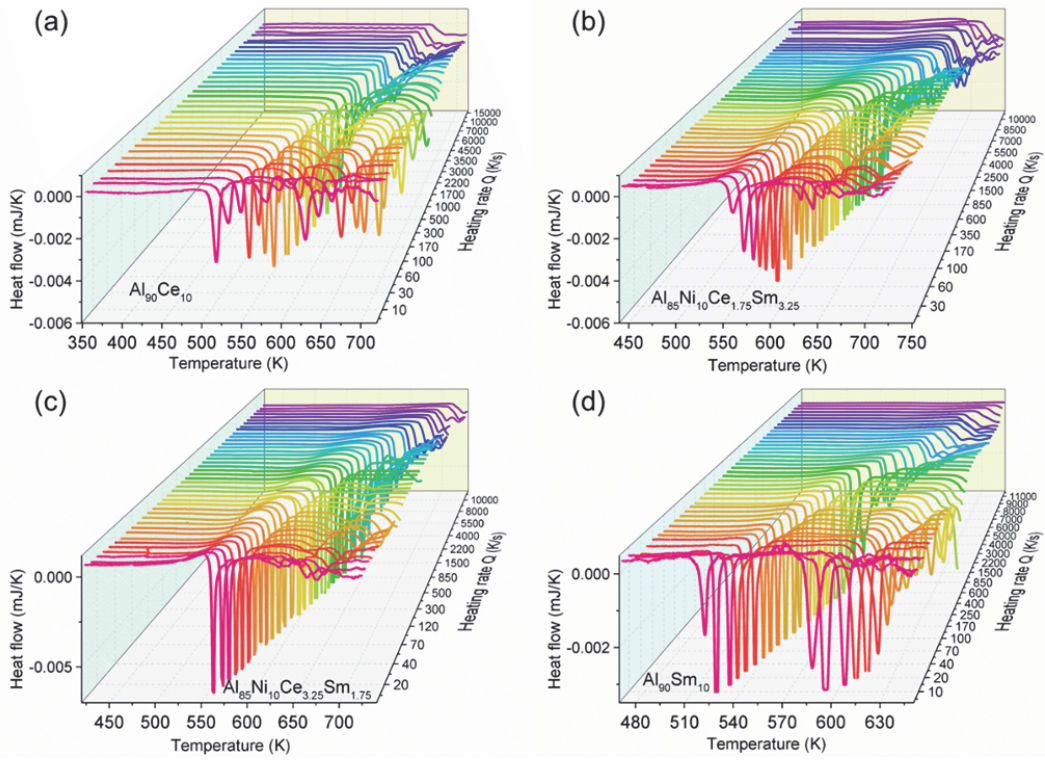


Figure S8. Heat flow curves are measured by FSC using different heating rates from 10-10000 K/s for different Al-based MGs **(a)** $\text{Al}_{90}\text{Ce}_{10}$; **(b)** $\text{Al}_{85}\text{Ni}_{10}\text{Ce}_{1.75}\text{Sm}_{3.25}$; **(c)** $\text{Al}_{85}\text{Ni}_{10}\text{Ce}_{3.25}\text{Sm}_{1.75}$; **(d)** $\text{Al}_{90}\text{Sm}_{10}$.

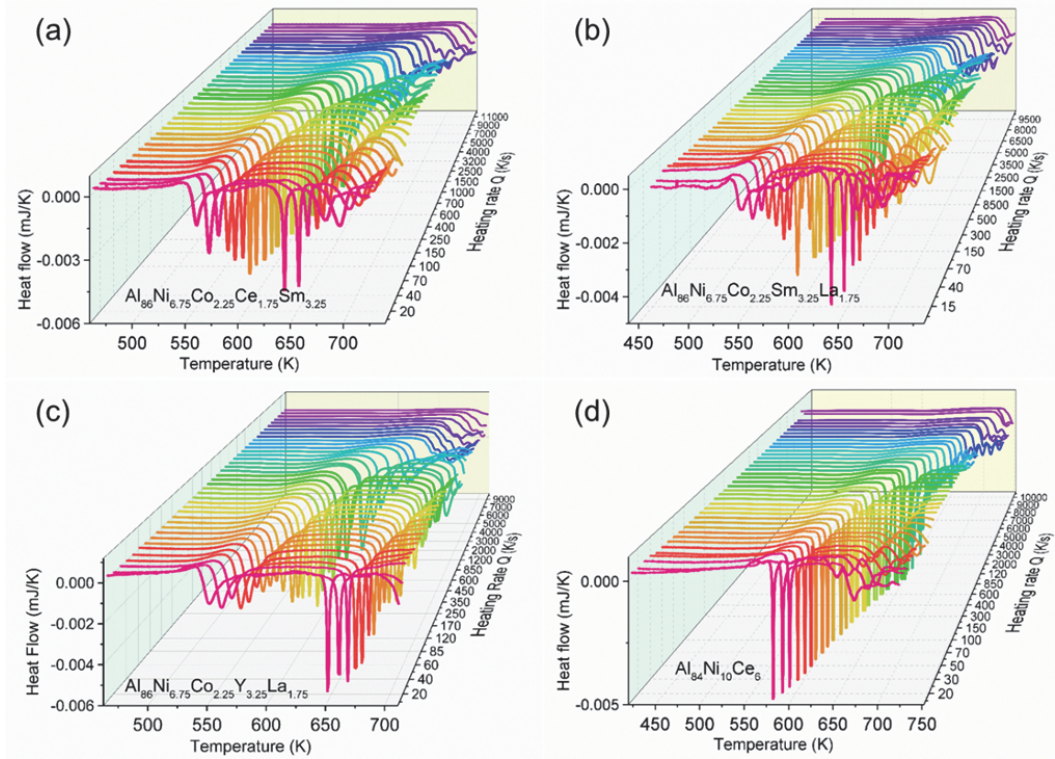


Figure S9. Heat flow curves are measured by FSC using different heating rates from 10-10000 K/s for different Al-based MGs **(a)** $\text{Al}_{86}\text{Ni}_{6.75}\text{Co}_{2.25}\text{Ce}_{1.75}\text{Sm}_{3.25}$; **(b)** $\text{Al}_{86}\text{Ni}_{6.75}\text{Co}_{2.25}\text{Sm}_{3.25}\text{La}_{1.75}$; **(c)** $\text{Al}_{86}\text{Ni}_{6.75}\text{Co}_{2.25}\text{Y}_{3.25}\text{La}_{1.75}$; **(d)** $\text{Al}_{84}\text{Ni}_{10}\text{Ce}_6$.

3. Detailed data on the glass forming ability (GFA) studied in this work for 20 typical Al-MGs with different compositions. Amorphous ribbons of different thicknesses was obtained by varying the rotational speed of the rollers at speeds between 10 m/s and 60 m/s. Subsequently, the amorphous nature of different thicknesses ribbons were investigated by X-ray diffraction (XRD, Bruke D2 Phaser) with monochromatic Cu K α radiation ($\lambda = 0.1542$ nm).

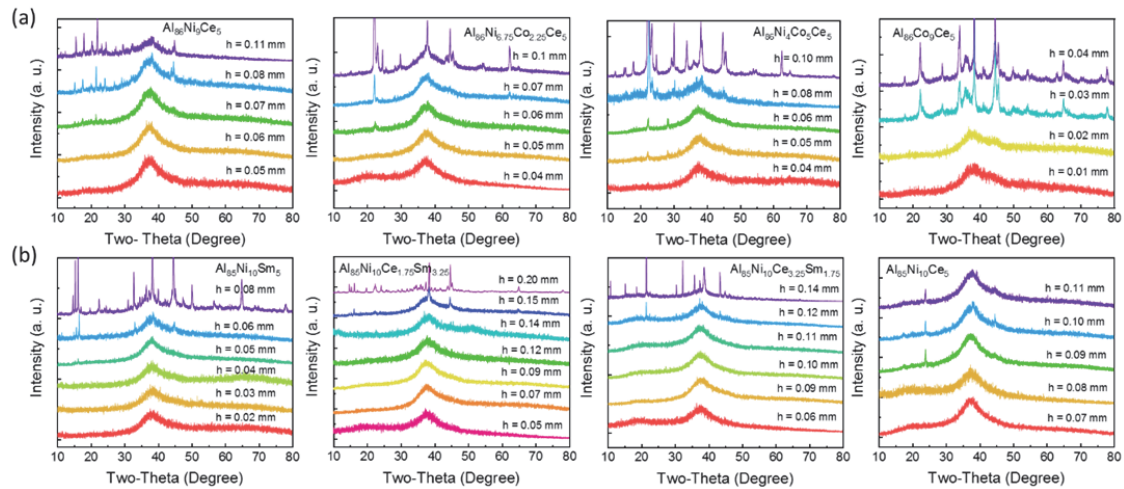


Figure S10. XRD patterns of ribbons with different thicknesses for different Al-based MGs **(a)** Al₈₆Ni_{9-x}Co_xCe₅ ($x=0, 2.25, 5, 9$ at.%) ; **(b)** Al₈₅Ni₁₀Sm_{5-x} ($x=0, 1.75, 3.25, 5$ at.%).

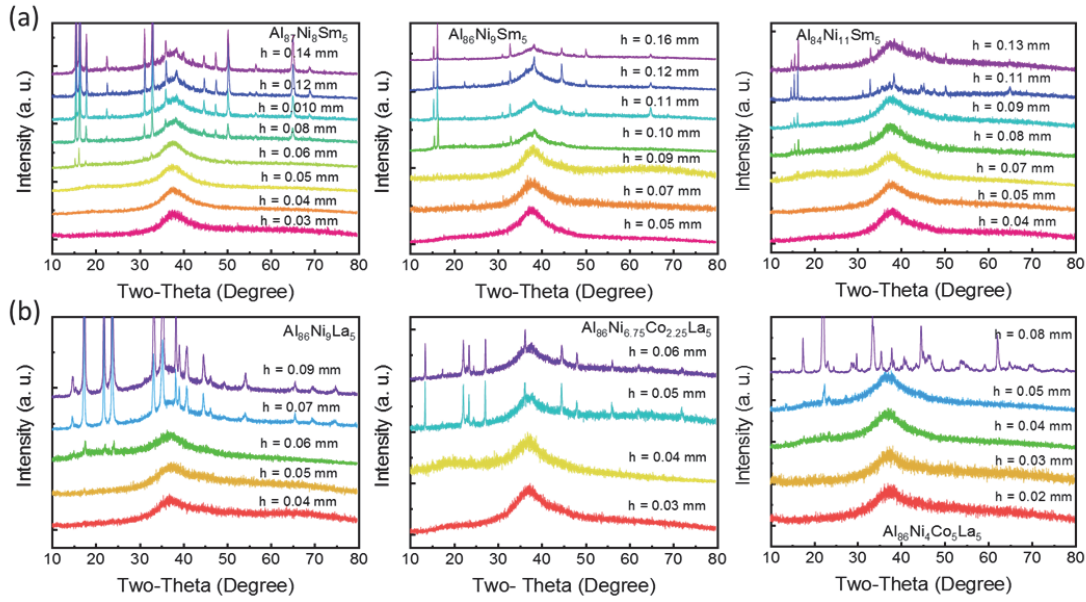


Figure S11. XRD patterns of ribbons with different thicknesses for different Al-based MGs **(a)** Al_{95-x}Ni_xSm₅ ($x = 8, 9, 11$ at.%) ; **(b)** Al₈₆Ni_{9-x}Co_xLa₅ ($x = 0, 2.25, 5$ at.%).

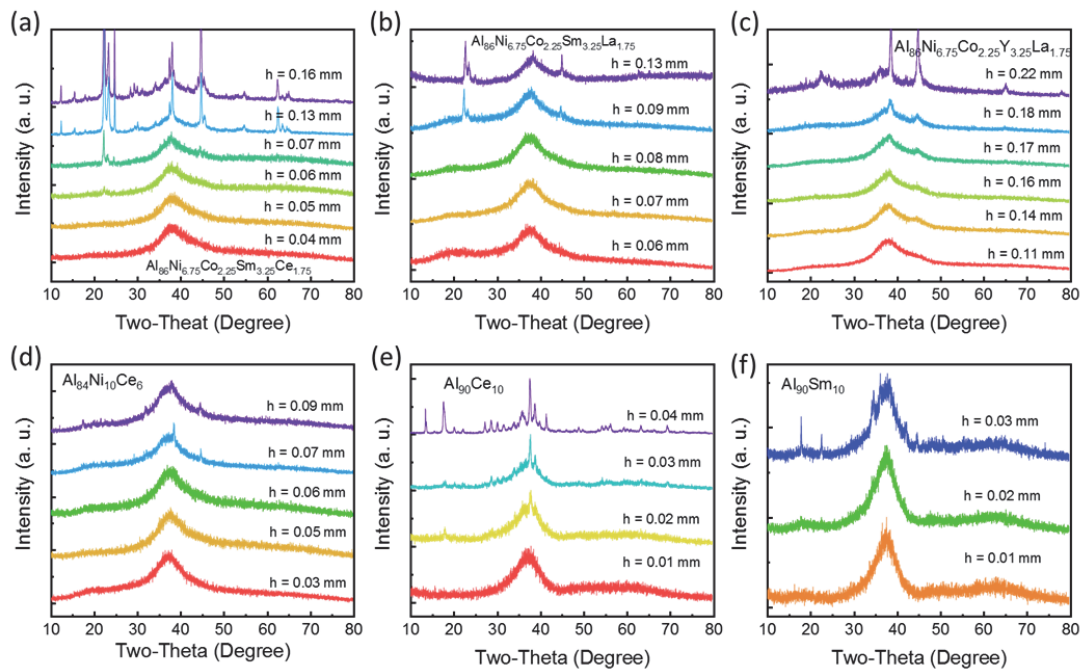


Figure S12. XRD patterns of ribbons with different thicknesses for different Al-based MGs **(a)** Al₈₆Ni_{6.75}Co_{2.25}Sm_{3.25}Ce_{1.75}; **(b)** Al₈₆Ni_{6.75}Co_{2.25}Sm_{3.25}La_{1.75}; **(c)** Al₈₆Ni_{6.75}Co_{2.25}Y_{3.25}La_{1.75}; **(d)** Al₈₄Ni₁₀Ce₆; **(e)** Al₉₀Ce₁₀; **(f)** Al₉₀Sm₁₀.

Al₈₆Ni_{6.75}Co_{2.25}Y_{3.25}La_{1.75}; (d) Al₈₄Ni₁₀Ce₆; (e) Al₉₀Ce₁₀; (f) Al₉₀Sm₁₀.

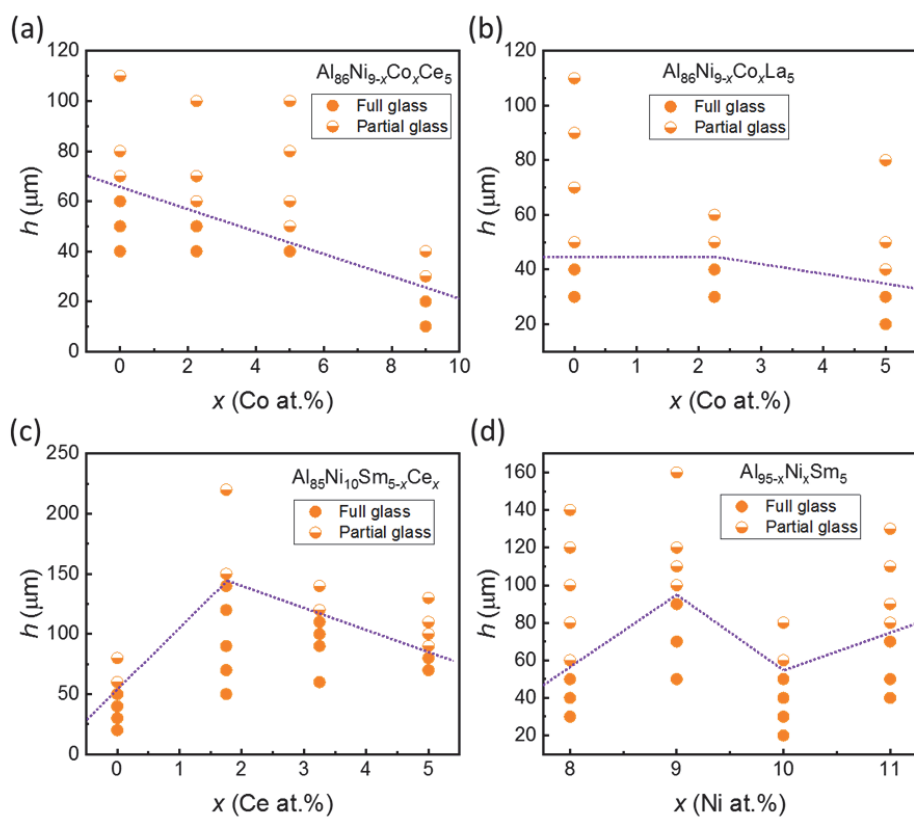


Figure S13. Illustration of glass formation range in different Al-based MGs system. **(a)**

Al₈₆Ni_{9-x}Co_xCe₅ ($x=0, 2.25, 5, 9$ at.%); **(b)** Al₈₆Ni_{9-x}Co_xLa₅ ($x=0, 2.25, 5$ at.%); **(c)**

$\text{Al}_{85}\text{Ni}_{10}\text{Ce}_x\text{Sm}_{5-x}$ ($x=0, 1.75, 3.25, 5$ at.%); **(d)** $\text{Al}_{95-x}\text{Ni}_x\text{Sm}_5$ ($x=8, 9, 10, 11$ at.%).

4. Determination of the crystal melting temperature T_m and the liquid temperature T_L from DTA data.

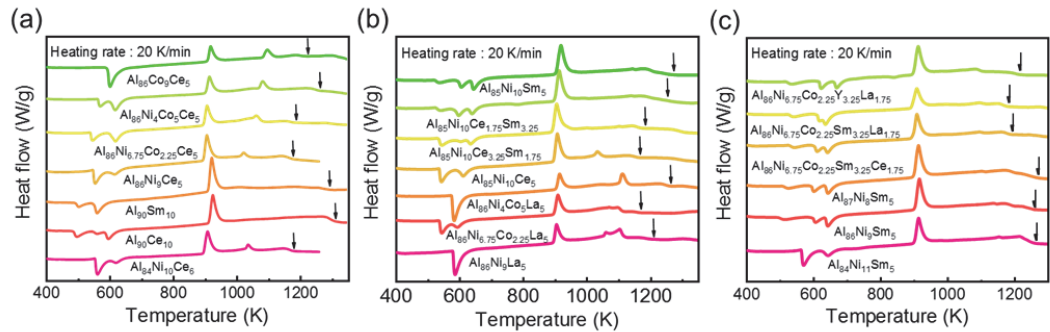


Figure S14. The heat flow curves measured by DTA (TA SDT Q600) with a heating rate of 20 K/min under a 100 ml/min argon gas flow for different Al-based MGs. The temperature marked by the black arrow is the liquid temperature T_L .

5. The database of liquid fragility and glass transition temperature for different glass formers with different bonding nature.

ID	Composition	T_g (K)	m	References
1	3-bromopentane	108	69	[1]
2	3-styrene	237	72	[1]
3	5-polyphenylether	248	85	[1]
4	2-phenyl-5-acetomethyl-5-ethyl-1,3-dioxocyclohexane	219	72	[1]
5	benzophenone	208	125	[1]
6	butyronitrile	97	56	[1]
7	biphenyl-2yl-isobutylate	209	77	[1]
8	3,3,4,4,-benzophenone-tetra-carboxylic dianhydride	333	80	[1]
9	isopropylbenzene-1	129	70	[1]
10	isopropylbenzene-2	129	73	[1]
11	dibutylammonium formate	155	57	[1]
12	dibutylphthalate	179	75	[1]
13	di-n-butylphthalate	168	69	[1]
14	tetraphenyl?tetramethyl trisiloxane	213	95	[1]
15	dichyclohexyl-methyl-2-methylsuccinate	221	76	[1]
16	diethylphthalate	185	70	[1]
17	decahydroisoquinoline	180	129	[1]
18	di-iso-butylphthalate	194	78	[1]
19	dimethylphthalate	195	70	[1]
20	dioctylphthalate	187	60	[1]
21	dipropylene glycol	196	66	[1]
22	dipropylglycol?dimethylether	136	78	[1]
23	ether-2-ethylhexylamine	140	71	[1]
24	ethanol	92.5	55	[1]
25	diglycidylether of bisphenol A (epoxy resin)	225	96	[1]
26	3-fluoroaniline	173	95	[1]
27	glycerol	191	53	[1]
28	cresolphthalein?dimethylether	318	73	[1]
29	m-tricresylphosphate	208	76	[1]
30	2-methyltetrahydrofuran-1	92	65	[1]
31	2-methyltetrahydrofuran-2	91	84	[1]
32	m-toluidine	185	77	[1]
33	n-propanol-1	99	40	[1]
34	n-propanol-2	99	35	[1]
35	o-terphenyl	243	81	[1]

36	phenolphthalein dimethylether	294	85	[1]
37	1,2-propandiol (propylene glycol)	164	52	[1]
38	perhydroisoquinoline	181	130	[1]
39	polypropylene glycol	199	75	[1]
40	pyridine?toluene	126	109	[1]
41	salol	221	73	[1]
42	sucrose benzonate	340	94	[1]
43	squalane	170	75	[1]
44	sorbitol	368	93	[1]
45	tri- α -naphthylbenzene-1	335	76	[1]
46	tri- α -naphthylbenzene-2	335	66	[1]
47	tricresylphosphate	209	76	[1]
48	trisnaphthylbenzene	342	86	[1]
49	toluene	166	105	[1]
50	tripropylene glycol	192	72	[1]
51	triphenyl phosphite	204	69	[1]
52	xylitol	250	87	[1]
53	ethyl benzene	115	98	[1]
54	toluene	117	105	[1]
55	Iso-propyl benzene	128	70	[1]
56	α -Picoline	129	72	[1]
57	propylene carbonate	157	99	[1]
58	4-tert-Butyl pyridine (4-TBP)	164	103	[1]
59	Propylene glycol	168	52	[1]
60	glycerol	188	53	[1]
61	dimethyl phthalate	191	70	[1]
62	monoepoxide phenyl glycidyl ether (PGE)	194	81	[1]
63	m-Tricresyl phosphate (m-TCP)	205	76	[1]
64	biphenyl	245	96	[1]
65	poly(vinyl acetate)	303	95	[1]
66	2-Methyl pentane	77	36	[2]
67	3-Bromopentane	108	53	[2]
68	2-Methyltetrahydrofuran	91	65	[2]
69	dibutyl phthalate	179	69	[2]
70	tris-naphthylbenzene	344.8	86	[2]
71	deuterated tris-naphthylbenzene	342.9	83	[2]
72	squalane	167.4	75	[2]
73	chiral isoocetylcyanobiphenyl	221	87	[2]
74	phenolphthalein dimethylether	294	75	[2]
75	1,1'-Bis(p-methoxyphenyl) cyclohexane	241	72	[2]
76	triphenylchloromethane	243	93	[2]

77	di-2-ethylhexylphthalate	187	67	[2]
78	m-Xylene	120	56	[2]
79	o-Xylene	123	55	[2]
80	a-phenyl-o-cresol	220	83	[2]
81	m-Fluorotoluene	117	45	[2]
82	5-Phenyl-4-ether	243	85	[2]
83	aroclor A 1248	229	85	[2]
84	bis-phenol-C-dimethylether	240	96	[2]
85	sucrose benzoate	337	94	[2]
86	cresolphthalein-dimethylether	314	68	[2]
87	decahydro-naphthalene	135	147	[2]
88	tri-2-naphthylbenzene	337	66	[2]
89	1,10-Di(4-methoxy-5-methylphenyl) cyclohexane	261	66	[2]
90	n-ethylacetamide	158.2	65	[2]
91	glycerol	186	48	[3]
92	m-toluidine	187	77	[3]
93	propanol	98	40	[3]
94	methanol	100	39	[4]
95	n-propanol	96.2	40	[4]
96	butyronitrile	97	56	[4]
97	ethylene glycol	151	50	[4]
98	m-cresol	198.6	57	[4]
99	b-D-fructose	286	61	[4]
100	phenolphthalein	363	62	[4]
101	Indomethacin	318	75	[4]
102	hydrochloro-thiazide	385	65	[4]
103	griseofulvin	364	65	[4]
104	1,3,5-tri--naphthylbenzene	340	76	[4]
105	diethylphthalate	178	73	[4]
106	probucol	295	67	[4]
107	9-bromophenanthrene	224.8	69	[4]
108	phenobarbital	319	70	[4]
109	d-glucose	309	72	[4]
110	maltitol	311	75	[4]
111	glibenclamide	331	75	[4]
112	flopropione	335	81	[4]
113	phenyl-cresol	220	61	[4]
114	sucrose	345	98	[4]
115	BSC	825	32	[1]
116	CN60.0	1030	27	[1]
117	CN60.2	820	22	[1]

118	CN60.4	700	19	[1]
119	NBS	705	32	[1]
120	NBS 710	830	35	[1]
121	NS 66	726	38	[1]
122	NS 80	758	37	[1]
123	PS1	738	19	[1]
124	PS2	746	18	[1]
125	PS3	765	20	[1]
126	Soda lime	536	40	[2]
127	NS75.6	764	30	[2]
128	NS75	739	37	[2]
129	NS67	729	45	[2]
130	$\text{CaAl}_2\text{Si}_2\text{O}_8$	1118	53	[2]
131	Silicate flint glass	538	57	[2]
132	$\text{Na}_2\text{O}\cdot 2\text{SiO}_2$	713	38	[2]
133	$70\text{SiO}_2\cdot 11\text{B}_2\text{O}_3\cdot 9\text{Na}_2\text{O}\cdot 7\text{K}_2\text{O}\cdot 3\text{BaO}$	860	32	[2]
134	$0.756\text{SiO}_2\cdot 0.244\text{K}_2\text{O}$	778	29	[2]
135	$0.756\text{SiO}_2\cdot 0.122\text{Na}_2\text{O}\cdot 0.122\text{K}_2\text{O}$	729	29	[2]
136	SiO_2	1500	20	[2]
137	Silica (infrasil)	1449	28	[2]
138	Borosilicate glass	795	26	[2]
139	Borosilicate BB	851	43	[2]
140	Borosilicate pyrex	871	31	[2]
141	Borosilicate E	996	33	[2]
142	Borosilicate BNC	850	37	[2]
143	Borosilicate NC	850	34	[2]
144	Soda lime silica	811	35	[2]
145	GeO_2	818	20	[2]
146	$\text{NaAlSi}_2\text{O}_6$	1053	29	[2]
147	B_2O_3	554	32	[2]
148	$\text{CaO}\cdot \text{MgO}\cdot 2\text{SiO}_2$	995	66	[5]
149	$\text{Na}_2\text{O}\cdot 2\text{SiO}_2$	708	29	[5]
150	$\text{Li}_2\text{O}\cdot 2\text{SiO}_2$	710	33	[5]
151	$\text{Na}_2\text{O}_2\cdot \text{SiO}_2$	728	36	[6]
152	$\text{Li}_2\text{O}\cdot 2\text{SiO}_2$	727	35	[6]
153	$\text{Li}_2\text{O}\cdot 2\text{B}_2\text{O}_3$	749	88	[6]
154	GeO_2	830	18	[6]
155	NIST 710a	831	45	[6]
156	E-glass	962	51	[6]
157	Basalt	943	63	[6]
158	$45\text{CaO}\cdot 55\text{SiO}_2$	1025	90	[6]

159	55CaO·45SiO ₂	1056	141	[6]
160	Fe ₈₃ B ₁₇	760	103	[7]
161	Au _{77.8} Ge _{13.8} Si _{8.4}	294	92	[7]
162	Fe _{41.5} Ni _{41.5} B ₁₇	720	99	[7]
163	Co ₇₅ Si ₁₅ B ₁₀	785	118	[7]
164	Fe ₇₉ Si ₁₀ B ₁₁	818	117	[7]
165	Ni ₇₅ Si ₈ B ₁₇	818	121	[7]
166	Fe ₈₀ P ₁₃ B ₇	736	102	[7]
167	Pt ₆₀ Ni ₁₅ P ₂₅	500	86	[7]
168	Pd ₈₂ Si ₁₈	657	106	[7]
169	Pd _{79.5} Cu ₄ Si _{16.5}	635	77	[7]
170	Ce ₇₀ Ni ₁₀ Cu ₁₀ Al ₁₀	359	37	[7]
171	Au ₄₉ Ag _{5.5} Pd _{2.3} Cu _{26.9} Si _{16.3}	401	70	[7]
172	Fe ₄₈ Cr ₁₅ Mo ₁₄ C ₁₅ B ₆ Y ₂	822	51	[7]
173	Pd ₇₇ Cu ₆ Si ₁₇	642	52	[7]
174	La ₅₅ Cu ₂₀ Al ₂₅	456	43	[7]
175	Pd _{77.5} Cu ₆ Si _{16.5}	637	73	[7]
176	La ₅₅ Ni ₂₀ Al ₂₅	491	35	[7]
177	Mg ₆₅ Cu ₂₅ Y ₁₀	413	46	[7]
178	Zr ₄₂ Cu ₄₆ Al ₇ Y ₅	672	49	[7]
179	La ₅₅ Ni ₅ Cu ₁₅ Al ₂₅	459	42	[7]
180	La ₅₅ Ni ₁₅ Cu ₅ Al ₂₅	474	37	[7]
181	Zr _{46.25} Ti _{8.25} Cu _{7.5} Ni ₁₀ Be _{27.5}	622	36	[7]
182	Fe ₄₈ Cr ₁₅ Mo ₁₄ Er ₂ C ₁₅ B ₆	844	38	[7]
183	La ₅₅ Al ₂₅ Ni ₁₀ Cu ₁₀	467	35	[7]
184	Zr ₅₅ Co ₂₅ Al ₂₀	753	65	[7]
185	Zr ₄₄ Ti ₁₁ Cu ₁₀ Ni ₁₀ Be ₂₅	625	41	[7]
186	Zr _{52.5} Cu _{17.9} Ni _{14.6} Al ₁₀ Ti ₅	674	51	[7]
187	Zr ₅₇ Cu _{15.4} Ni _{12.6} Al ₁₀ Nb ₅	682	71	[7]
188	Pd ₄₈ Ni ₃₂ P ₂₀	590	43	[7]
189	Zr _{46.75} Ti _{8.25} Cu _{7.5} Ni ₁₀ Be _{27.5}	590	46	[7]
190	Zr ₄₅ Cu ₄₆ Al ₇ Y ₂	693	72	[7]
191	Zr _{58.5} Cu _{15.6} Ni _{12.8} Al _{10.3} Nb _{2.8}	660	46	[7]
192	Zr ₆₅ Cu _{17.5} Ni ₁₀ Al _{7.5}	656	35	[7]
193	Zr _{41.2} Ti _{13.8} Cu _{12.5} Ni ₁₀ Be _{22.5}	623	50	[7]
194	Mg ₆₅ Cu ₂₅ Gd ₁₀	423	39	[7]
195	Mg ₆₅ Cu ₂₀ Ni ₅ Gd ₁₀	423	39	[7]
196	Pd ₄₀ Cu ₃₀ Ni ₁₀ P ₂₀	578	52	[7]
197	Pd _{42.5} Cu ₃₀ Ni _{7.5} P ₂₀	566	58	[7]
198	Pd _{42.5} Cu ₃₀ Ni _{7.5} P ₂₀	576	40	[7]
199	Pd ₄₃ Cu ₂₇ Ni ₁₀ P ₂₀	576	58	[7]

200	Zr ₅₅ Co ₂₅ Al ₂₀	753	65	[7]
201	Pd _{77.5} Cu ₆ Si _{16.5}	637	73	[7]
202	Cu ₄₇ Ti ₃₄ Zr ₁₁ Ni ₈	673	59	[5]
203	La ₅₅ Cu ₂₀ Al ₂₅	456	42	[5]
204	La ₅₅ Cu ₁₀ Ni ₅ Co ₅ Al ₂₅	466	37	[5]
205	Zr ₆₅ Al _{7.5} Ni ₁₀ Cu _{17.5}	656	35	[5]
206	Pt _{57.5} Ni _{5.3} Cu _{14.7} P _{22.5}	490	68	[8]
207	Ce ₇₀ Ni ₁₀ Cu ₁₀ Al ₁₀	359	21	[8]
208	Pr ₆₀ Ni ₁₀ Cu ₁₀ Al ₁₀	409	31	[8]
209	Pr ₅₅ Co ₂₀ Al ₂₅	509	38	[8]
210	Tb ₅₅ Co ₂₀ Al ₂₅	612	32	[8]
211	Dy ₅₅ Co ₂₀ Al ₂₅	635	30	[8]
212	Ho ₅₅ Co ₂₀ Al ₂₅	649	25	[8]
213	Er ₅₅ Co ₂₀ Al ₂₅	663	28	[8]
214	Ca ₆₅ Li _{9.96} Mg _{8.54} Zn _{16.5}	317	20	[8]
215	Ni ₆₀ Nb ₃₅ Sn ₅	882	60	[8]
216	Mg ₆₅ Cu ₂₅ Tb ₁₀	428	47	[9]
217	Ni ₆₄ Pd ₁₆ P ₂₀	567	65	[10]
218	Pd ₆₄ Ni ₁₆ P ₂₀	582	67	[10]
219	Ni _{59.5} Nb _{40.5}	920	136	[9]
220	Ni ₆₉ Cr _{8.5} Nb ₃ P _{19.5}	660	100	[10]
221	Ni ₆₉ Cr _{8.5} Nb ₃ P ₁₈ B _{1.5}	664	77	[10]
222	Ni ₆₉ Cr _{8.5} Nb ₃ P _{16.5} B ₃	668	59	[10]
223	Ni ₆₉ Cr _{8.5} Nb ₃ P _{13.5} B ₆	671	54	[10]
224	Ni ₈₀ P ₂₀ ribbons	581	94	[10]
225	Fe _{74.5} Mo _{5.5} P _{12.5} C ₅ B _{2.5}	695	63	[10]
226	Fe ₆₈ Mo ₅ Ni ₅ Cr ₂ P _{12.5} C ₅ B _{2.5}	668	62	[10]
227	Fe ₄₈ Cr ₁₅ Mo ₁₄ C ₁₅ B ₆ Y ₂	822	51	[10]
228	Fe ₄₁ Co ₇ Cr ₁₅ Mo ₁₄ C ₁₅ B ₆ Y ₂	820	43	[10]
229	Pd _{79.5} Au ₄ Si _{16.5}	620	77	[10]
230	Pd ₄₀ Ni ₄₀ P ₁₉ Si ₁	567	48	[10]
231	Zr ₅₀ Cu ₅₀	673	58	[10]
232	Zr ₁₁ Ti ₃₄ Cu ₄₇ Ni ₈	671	67	[10]
233	Zr ₅₇ Nb ₅ Cu _{15.4} Ni _{12.6} Al ₁₀	674	48	[10]
234	Zr _{58.5} Nb _{2.8} Cu _{15.6} Ni _{12.8} Al _{10.3}	666	48	[10]
235	Mg _{59.4} Cu ₂₃ Ag _{6.6} Gd ₁₁	425	44	[10]
236	Zr ₅₅ Co _{22.5} Al _{22.5}	753	73	[2]
237	Pd ₄₀ Ni ₄₀ P ₂₀	560	51	[2]
238	Pt ₄₅ Ni ₃₀ P ₂₅	482	48	[2]
239	Pt ₆₀ Ni ₁₅ P ₂₀	482	50	[2]
240	Pr ₆₀ Cu ₂₀ Ni ₁₀ Al ₁₀	409	31	[2]

241	(Fe ₅ Co ₆₃ B ₁₂) ₈₀ Si ₃ Al ₅ Ga ₂ P ₁₀	745	63	[2]
242	Fe ₈₀ P ₁₃ C ₇	736	102	[2]
243	Ni _{62.4} Nb _{37.6}	945	121	[2]
244	Ce ₇₀ Ni ₁₀ Cu ₁₀ Al ₁₀	359	21	[2]
245	Pd ₇₇ Cu ₆ Si ₁₇	635	52	[2]
246	Pd ₄₃ Ni ₁₀ Cu ₂₇ P ₂₀	569	65	[2]
247	Gd ₅₅ Al ₂₅ Cu ₁₀ Co ₅ Ni ₅	563	37	[11]
248	Gd ₅₅ Al ₂₅ Co ₁₉ Cu ₁₀	563	45	[11]
249	Gd ₅₅ Al ₂₅ Ni ₁₀ Co ₁₀	579	58	[11]
250	Gd ₅₅ Al ₂₅ Co ₂₀	589	74	[11]
251	Ca ₆₅ Mg ₁₅ Zn ₂₀	373	21	[12]
252	Ce ₇₀ Ni ₁₀ Cu ₁₀ Al ₂₀	358	29	[12]
253	Hf ₅₀ Ni ₂₅ Al ₂₅	858	33	[12]
254	Hf ₅₅ Ni ₂₅ Al ₂₀	828	36	[12]
255	La ₆₆ Cu ₁₀ Ni ₁₀ Al ₁₄	459	32	[12]
256	Fe ₆₃ Mo ₁₄ C ₁₅ B ₆ Er ₂	778	28	[12]
257	Fe ₆₅ Mo ₁₄ C ₁₅ B ₆	790	33	[12]
258	Pt _{57.5} Cu _{14.7} Ni _{5.3} P _{22.5}	508	68	[12]
259	Pd _{77.5} Cu ₆ Si _{16.5}	673	52	[12]
260	Mg ₆₅ Cu _{7.5} Ni _{7.5} Zn ₅ Ag ₅ Y ₅ Gd ₅	431	40	[12]
261	Mg ₆₅ Cu ₂₅ Gd ₁₀	423	39	[12]
262	Mg _{58.5} Cu _{30.5} Y ₁₁	412	30	[12]
263	Mg ₅₇ Cu ₃₁ Y _{6.6} Nd _{5.4}	427	29	[12]
264	Cu _{47.5} Zr _{47.5} Al ₄	683	44	[12]
265	Cu ₄₃ Zr ₄₃ Al ₇ Ag ₇	700	45	[12]
266	Cu ₄₃ Zr ₄₃ Al ₇ Be ₇	696	42	[12]
267	Cu _{46.25} Zr _{45.25} Al _{7.5} Sn ₁	718	40	[12]
268	Cu ₅₀ Zr ₅₀	664	39	[12]
269	Zr ₄₂ Cu ₄₆ Al ₇ Y ₅	713	49	[12]
270	Zr ₆₄ Cu ₂₆ Al ₁₀	662	44	[12]
271	Zr ₅₀ Cu _{41.5} Al _{5.5} Mo ₃	688	50	[12]
272	Zr ₅₀ Cu ₄₃ Al _{5.5} Mo _{1.5}	685	47	[12]
273	Zr ₅₀ Cu ₄₄ Al _{5.5} Mo _{0.5}	682	41	[12]
274	Zr ₅₀ Cu _{44.5} Al _{5.5}	678	39	[12]
275	Zr ₆₀ Cu ₄₈ Al ₁₂	676	47	[12]
276	Zr ₆₂ Cu ₂₃ Al ₇ Pb ₅ Nb ₃	670	56	[12]
277	Zr ₆₀ Cu ₂₅ Al ₇ Pb ₅ Nb ₃	674	43	[12]
278	Zr ₅₅ Cu ₃₀ Al ₇ Pb ₅ Nb ₃	693	41	[12]
279	Zr ₅₀ Cu ₃₅ Al ₇ Pb ₅ Nb ₃	710	37	[12]
280	Pr ₅₅ Ni ₂₅ Al ₂₀	484	19	[13]
281	Sm ₅₅ Co ₁₀ Cu ₁₀ Al ₂₅	534	27	[13]

282	$\text{Sm}_{50}\text{Co}_{20}\text{Al}_{30}$	586	29	[13]
283	$\text{Ce}_{55}\text{Al}_{45}$	541	32	[13]
284	$\text{Sm}_{55}\text{Ni}_{10}\text{Co}_{10}\text{Al}_{25}$	553	37	[13]
285	$\text{Pd}_{36.5}\text{Ni}_{36.5}\text{P}_{27}$	635	62	[14]
286	$\text{Pd}_{37.5}\text{Ni}_{37.5}\text{P}_{25}$	619	51	[14]
287	$\text{Fe}_{30.8}\text{Co}_{46.2}\text{P}_{14}\text{B}_6\text{Al}_3$	724	43	[14]
288	$\text{Pt}_{64}\text{Ni}_{16}\text{P}_{20}$	482	50	[14]
289	$\text{Pt}_{56}\text{Ni}_{14}\text{P}_{30}$	498	56	[14]
290	$\text{Au}_{76.9}\text{Ge}_{13.65}\text{Si}_{19.45}$	295	60	[14]
291	$\text{Ni}_{75}\text{P}_{16}\text{B}_6\text{Al}_3$	691	53	[10]
292	$\text{Zr}_{60}\text{Cu}_{40}\text{Al}_{10}$	706	57	[10]
293	$\text{Mg}_{61}\text{Cu}_{28}\text{Gd}_{11}$	418	38	[10]

References for Supplementary Material

- [1] A. Jaiswal, T. Egami, K. F. Kelton, K. S. Schweizer, and Y. Zhang, Correlation between Fragility and the Arrhenius Crossover Phenomenon in Metallic, Molecular, and Network Liquids, *Phys. Rev. Lett.* **117**, 205701 (2016).
- [2] Q. Qin and G. B. McKenna, Correlation between dynamic fragility and glass transition temperature for different classes of glass forming liquids, *J. Non-Cryst. Solids* **352**, 2977 (2006).
- [3] V. N. Novikov, Y. Ding, and A. P. Sokolov, Correlation of fragility of supercooled liquids with elastic properties of glasses, *Phys. Rev. E* **71**, 061501 (2005).
- [4] L. M. Wang, C. A. Angell, and R. Richert, Fragility and thermodynamics in nonpolymeric glass-forming liquids, *J. Chem. Phys.* **125**, 074505 (2006).
- [5] O. N. Senkov, Correlation between fragility and glass-forming ability of metallic alloys, *Phys. Rev. B* **76** (2007).
- [6] L. Hornbøll and Y. Yue, Enthalpy relaxation in hyperquenched glasses of different fragility, *J. Non-Cryst. Solids* **354**, 1862 (2008).
- [7] X.-J. Xu, Z.-L. Long, W. Liu, and G.-K. Liao, Effects of fragility and reduced glass

transition temperature on the glass formation ability of amorphous alloys, Mater. Res. Exp. **4**, 115201 (2017).

[8] W. H. Wang, The elastic properties, elastic models and elastic perspectives of metallic glasses, Prog. Mater. Sci. **57**, 487 (2012).

[9] V. N. Novikov and A. P. Sokolov, Correlation of fragility and Poisson's ratio: Difference between metallic and nonmetallic glass formers, Phys. Rev. B **74** (2006).

[10] W. L. Johnson, J. H. Na, and M. D. Demetriou, Quantifying the origin of metallic glass formation, Nat. Commun. **7**, 10313 (2016).

[11] J. Guo, X. Bian, Y. Zhao, S. Zhang, T. Li, and C. Wang, Correlation between the fragility of supercooled liquids and thermal expansion in the glassy state for Gd-based glass-forming alloys, J. Phys.: Condens. Matter **19**, 116103 (2007).

[12] T. Wang, L. Hu, Y. Liu, and X. Hui, Intrinsic correlation of the plasticity with liquid behavior of bulk metallic glass forming alloys, Mater. Sci. Eng. A **744**, 316 (2019).

[13] Q. Sun, C. Zhou, Y. Yue, and L. Hu, A Direct Link between the Fragile-to-Strong Transition and Relaxation in Supercooled Liquids, J. Phys. Chem. Lett. **5**, 1170 (2014).

[14] L. Hu, X. Bian, W. Wang, G. Liu, and Y. Jia, Thermodynamics and dynamics of metallic glass formers: their correlation for the investigation on potential energy landscape, J. Phys. Chem. B **109**, 13737 (2005).